Journal of Catalysis **197,** 81–90 (2001)
doi:10.1006/jcat.2000.3057, available online at http://www.idealibrary.com on IDEAL®

Al-ITQ-7, a Shape-Selective Zeolite for Acylation of 2-Methoxynaphthalene

P. Botella, A. Corma,[1] and G. Sastre

Instituto de Tecnología Química, UPV-CSIC, Universidad Politécnica de Valencia, Avda. de los Naranjos s/n, 46022 Valencia, Spain
E-mail: acorma@itq.upv.es

Received May 16, 2000; revised August 29, 2000; accepted August 29, 2000

Acylation of 2-methoxynaphthalene with acetic anhydride has been carried out with a tridirectional 12-member ring pore zeolite named ITQ-7, which has a slightly smaller pore diameter than zeolite Beta. ITQ-7 is as active as Beta but gives better selectivity to 2-acetyl-6-methoxynaphthalene (2-AMN). This is due to the differences in the relative diffusion coefficients of 2-AMN and 1-acetyl-2-methoxynaphthalene (1-AMN), whose ratios are 2.7 and 15.5 in Beta and ITQ-7, respectively. In general, it can be said that when decreasing the zeolite crystallite size, the reaction rate increases, although the selectivity to 2-AMN decreases. © 2001 Academic Press

Key Words: **acylation; 2-methoxynaphthalene; acetic anhydride; Beta; ITQ-7; molecular dynamics.**

INTRODUCTION

Aromatic ketones are used in the preparation of fine chemicals, and in this sense some fragrances and the production of anti-inflammatories of the Naproxen type include the acylation of aromatics in one of the reaction steps. Acylations are generally carried out using Friedel–Crafts catalysts, for instance, $AlCl_3$. Acetonaphthones were already being prepared in this way almost 70 years ago by reacting the corresponding aromatics with methoxy or ethoxy groups with the corresponding acyl chlorides, using $AlCl_3$ as a catalyst (1). The use of $AlCl_3$ as a catalyst for acylation reactions continues at present, despite, the fact that $AlCl_3$ is used in excess of the stoichiometric requirements, and HCl and polyoxo–aluminum complexes, which are difficult to separate, are generated as subproducts. Nevertheless, environmental pressure is pushing this process toward the development of environmentally friendly solid acid catalysts that can be regenerated and recycled and can carry out the acylation reactions using more friendly anhydrides or even organic acids as acylation reagents. Among the different solid acids, zeolites have been proven to be good acylation catalysts with either acyl chlorides or anhydrides (2–7). Indeed, acylation of anisole by Y and Beta zeolites was already known to occur with good yields and selectivity (5–7), with Beta giving the best results. Further efforts on the catalyst and especially on the process design should result in the successful commercial acylation of anisole and veratrol using, respectively, Beta and Y zeolites (8, 9).

It would be of special interest to develop a highly active catalyst for the selective acylation of 2-methoxynaphthalene (2-MN) with acetic anhydride or acid at the 6-position, in this way producing 2-acetyl-6-methoxynaphthalene (2-AMN), which is an intermediate for the preparation of Naproxen (10). An important work on the preparation of 2-AMN using zeolites as catalysts was carried out by HOECHST (11). In this work the authors studied the acylation of 2-MN by anhydrides and acid chlorides on a series of zeolites such as HEU-1, Beta, and ZSM-12 using a ratio of 2-MN to acetic anhydride of 1 : 3, at temperatures up to 573 K. They found that with acetyl chloride and acetic anhydride the ratio of 2-AMN to 1-AMN (1-acetyl-2-methoxynaphthalene) was always lower than 1, and only when propionic anhydride was used was the ratio of 2-AMN to 1-AMN higher than 1, especially when using ZSM-12 as the catalyst. Other zeolites such as faujasites (10, 12), Beta (10, 12–14), mordenite (12), and mesoporous molecular sieves (15) have also been studied as catalysts for the acylation of 2-MN. Even if the acylation occurs preferentially at the kinetically controlled 1-position of the 2-MN molecule, with the formation of 1-AMN the pore dimensions of the zeolite can introduce shape selectivity effects which can change the 2-AMN to 1-AMN yield ratio in the products. In this sense, the Beta zeolite seems to have good pore dimensions favoring the diffusion of the 2-AMN molecule with respect to the 1-AMN isomer (10, 14, 16). However, it should be considered that, while there are some authors which claim that 1-AMN can only be formed at the external surface of the Beta zeolite (13, 14), others claim that the bulkier isomer can also be formed within the pores and that a transacylation mechanism between 1-AMN and 2-MN molecules is the essential step for 2-AMN formation (17).

---

[1] To whom correspondence should be addressed.

0021-9517/01 $35.00

It appeared to us that a large-pore tridirectional zeolite with slightly smaller pores than those of Beta zeolites could be even more selective toward the formation of 2-AMN. Very recently, a new tridirectional large-pore zeolite named ITQ-7 (Instituto de Tecnología Química-7) has been synthesized in the pure silica form (18) and in its acid form (19). This zeolite has two channels with 6.2 × 6.1 Å and a third of 6.3 × 6.1 Å which are smaller than the two major channels of the Beta zeolite, 7.2 × 6.2 Å, since the third one in Beta (5.5 × 5.5 Å) is not of use for the acylation reaction. In this work we have studied the acylation of 2-MN with acetic anhydride using Al-ITQ-7 as a catalyst. The influence of zeolite crystallite size on activity and selectivity toward the 2-AMN isomer has been investigated and the results have been compared with those of Beta zeolites with different compositions and crystal sizes. A higher selectivity to 2-AMN has been observed with the Al-ITQ-7 zeolite, and the results are explained on the basis of different diffusion of the two isomers in Beta and Al-ITQ-7. This assumption is supported by Molecular Dynamics calculations, which have been performed to simulate the diffusion of 2-methoxynaphthalene and the acylated 1-AMN and 2-AMN products in Beta and Al-ITQ-7 zeolites.

EXPERIMENTAL

Materials

Two commercial zeolite samples were provided by P.Q. Industries: a Beta zeolite (CP811) and a USY zeolite (CBV760). SSZ-33 (20), UTD-1 (21), and Beta samples (22) were synthesized in our laboratory. Beta 1, 2, and 4 samples (small crystal) were prepared by a seeding process, using nanocrystalline Beta zeolite as seed. Beta 3 (large crystal) was made without seeding. ITQ-7 samples were prepared in a fluoride medium as B-ITQ-7 (19). These zeolites were exchanged with a solution of $Al(NO_3)_3$ in order to obtain the corresponding Al-ITQ-7, following the method indicated by Lobo and Davis (23).

The Al content in the samples was determined by atomic absorption spectrophotometry (Varian spectrAA-10 Plus). Crystallinity was measured by powder X-ray diffraction, using a Phillips PW1710 diffractometer with Cu $K\alpha$ radiation, and comparison with a highly crystalline standard sample. The acidity of the samples was established by the standard pyridine adsorption–desorption method (24). The surface area of the catalysts was calculated by the BET/BJH method with N_2 adsorption/desorption performed at 77 K in a Micromeritics ASAP 2000 instrument. The crystal size was determined from the SEM images obtained in a JEOL 6300 scanning electron microscope.

The most relevant physicochemical properties of these zeolites are summarized in Table 1.

Reaction Procedure

Experiments were made in a 25-ml three-neck round-bottom flask, connected to a reflux cooler system, at 405 K under an argon atmosphere and with magnetic stirring. All reagents were supplied by Aldrich. The standard conditions were the following: 100–200 mg of catalyst were activated "*in situ*" before the reaction by heating for 2 h at 573 K in a vacuum. Then, a mixture of 4.0 mmol of 2-methoxynaphthalene, 2.0 mmol of acid anhydride (AA), and 3 ml of chlorobenzene was added (2-MN/AA molar ratio = 2; catalyst/AA ratio = 1 g : 10–20 mmol acid

TABLE 1

Physicochemical Characteristics of Catalysts Tested in This Work

				Acidity (μmol py)[c]					
				Brönsted			Lewis		
Sample	Si/Al[a]	Area BET ($m^2 g^{-1}$)	Crystal size (μm)[b]	523 K	623 K	673 K	523 K	623 K	673 K
CP811	12.5	570	0.1–0.2	45	27	16	48	40	40
Beta 1	25	534	0.3–0.5	37	23	7	16	15	15
Beta 2	50	488	0.3–0.5	21	18	5	10	8	4
Beta 3	50	498	1–2	25	24	12	10	4	3
Beta 4	93	463	0.3–0.5	11	10	2	5	4	2
CBV760	27.5	551	0.4–0.6	14	3	1	10	7	4
SSZ-33	50	521	1 × 0.1 × 0.1	92	78	54	11	8	7
UTD-1	80	305	0.5	7	3	1	7	5	5
Al-ITQ-7	50	478	1.2	27	26	16	24	22	19
Al-ITQ-7n	75	317	0.02–0.05	6	3	2	13	6	5

[a] As-made molar ratio.

[b] Average size determined from the SEM images.

[c] Determined from the infrared spectra of adsorbed pyridine after evacuation at 523, 623, and 673 K.

anhydride). Small samples were taken periodically during 4 h. Upon recycling the catalyst, it was observed that some deactivation occurs during the reaction. Then, in all experiments, a large number of samples were taken during the first hour of reaction. Products were analyzed by GC in a Varian 3350 Series instrument equipped with a 30-m capillary cross-linked 5% phenylmethylsilicone column (HP-5) and a FID detector, using nitrobenzene as internal standard. Products were also identified by mass spectrometry in a Varian Saturn II GC-MS model working with a Varian Star 3400 gas chromatograph and using reference samples.

Conversion of 2-MN has been referred to the maximum conversion possible, while the selectivity to the different products has been indicated according to the methoxyacetonaphthones distribution. Moreover, coke-like products were formed on the catalyst during the reaction, and this became dark-brown. Catalysts were extracted in a microsoxhlet with $CHCl_3$ during 12 h. The solvent was evaporated and the remaining organic material was weighted, diluted with chlorobenzene, and analyzed by GC-MS. Among the adsorbed products we found acetic acid, 2-MN, and methoxyacetonaphthones. Although their percentages were usually less than 1 wt%, they were considered for the calculation of the total mass balance. Carbon content in the used catalyst was determined to quantify the nonextractable organic deposit by thermogravimetric and C-elemental analysis performed, respectively, in a NEST instrument using calcined kaolin as reference material and in a FISONS EA 1108 CHSN-O apparatus. Ultraviolet-visible spectroscopy (Varian Cary 5G UV-VIS-NIR spectrophotometer) was used to study the nature of functional groups present in the coke. Taking into account all of these fractions it was possible to obtain mass balances $\geq$98%.

Molecular Dynamics Methodology

Periodic atomistic Molecular Dynamics (MD) calculations have been performed to simulate the diffusion of 2-MN, and the acetilated products in positions 1 and 6, 1-AMN, and 2-AMN, in purely siliceous Beta and ITQ-7. The purely siliceous unit cells of Beta and ITQ-7 (IZA codes BEA and ISV, respectively, see Ref. 25) contain 192 atoms (64 SiO_2), and in order to have a larger number of atoms for the MD simulations, $3 \times 3 \times 2$ macrocells containing 3456 atoms were used. Thirteen molecules of adsorbate were located in the void space of the macrocell in order to complete the system. A total of six simulations was carried out, corresponding to 2-methoxynaphthalene, 1-AMN, and 2-AMN in each of the two zeolitic structures.

The zeolite framework with the corresponding sorbate was first optimized using the BFGS (26) technique implemented in the GULP (27) code. This calculation gives a more reliable cell size which experiences a certain change after interaction with the corresponding sorbate and also allows the sorbates to relax their geometry inside the corresponding void space, thus allowing a better initial configuration for the MD run. The result is used as input for a 25-ps equilibration stage of the zeolite + sorbate system. After this period, runs of 400 ps, with a timestep of 1 fs, were carried out within a NVE microcanonical ensemble at 450 K. The temperature was equilibrated according to the Berendsen algorithm (28). The simulations proceed by first assigning initial velocities to all atoms according to a Maxwell–Boltzmann distribution which depends on the temperature of the system. From this starting point, Newton's equations of motion are solved using a finite time step by means of the standard Verlet algorithm (29).

In all simulations, every atom was allowed to move explicitly. Although this increases substantially the computational expense, the influence of the framework flexibility has been made clear in a number of studies (30–32), especially when the sorbate matches the pore dimensions, as is the case here. The MD simulations have been carried out using the general purpose DL_POLY_2.11 parallel code (33), which was installed on a CRAY-T3E computer at the CIEMAT. The simulations were run using 16 processors.

During the simulation, history files were saved every 100 steps, and subsequent analysis used the MSD (mean square displacements) facility included in DL_POLY to obtain mean square displacements. The expression used to calculate the MSD plots was (34)

$$\langle X^2(t)\rangle = 1/(N_\mathrm{m}\cdot N_\mathrm{to})\sum_\mathrm{m}\sum_{\mathrm{t_o}}[X_i(t+t_0)-(X_i(t_0))]^2, \quad [1]$$

where N_m is the number of diffusing molecules, N_to is the number of time origins used in calculating the average, and X_i is the coordinate of the center of mass of molecule i.

The diffusion coefficients, D, were then calculated using the Einstein relation (34),

$$\langle X^2(t)\rangle = 6\cdot D\cdot t + B, \quad [2]$$

where t is the simulation time, and B is the thermal factor arising from atomic vibrations.

The trajectories followed by the molecules in their diffusion path through the zeolite structures are visualized by means of the "*xz*" and "*yz*" projections, which highlight motion in the different 12-MR (member rings) channels present in Beta and ITQ-7. The *trajectory graphs* contain all the visual information needed to understand, at first sight, the basic mechanism of the diffusion process, and they allow us to see how the molecules diffuse through the channels.

Interatomic potentials. Four types of interatomic potentials are needed to model this system:

$$V_\mathrm{total} = V_\mathrm{zeolite} + V_\mathrm{sorbate} + V_\mathrm{sorbate-sorbate} + V_\mathrm{zeolite-sorbate}. \quad [3]$$

The potential for the framework, $V_\mathrm{zeolite,}$ was originally derived by Catlow *et al.* (35) and is essentially a Born model potential comprising three-body and short-range terms and long-range Coulomb interactions. The potential for the sorbates, V_{sorbate}, was taken from Oie *et al.* (36) and comprises two- (bond), three- (angle), and four-body (dihedral) interactions together with Coulomb terms. Finally, 12-6 Lennard–Jones potentials, taken from Catlow *et al.* (35), and Coulomb interactions were used to describe the sorbate–sorbate and framework–sorbate interactions. The charges for the sorbates were taken from a Hartree–Fock calculation using the 6-31G** basis set (37). The charges of the sorbate atoms were then scaled by a factor of 0.6 to decrease the effect of the fully ionic zeolite framework and make the coulombic interaction of zeolite–sorbate more reliable. This procedure has been successfully used earlier (38). More details regarding the potential parameters (39) and the techniques employed can be found in previous studies (40–44).

RESULTS AND DISCUSSION

During the acylation of 2-MN with acetic anhydride it has been found (45) that both isomers, 1-AMN and 2-AMN, are formed as primary products. However, acylation occurs preferentially at position 1, which is the kinetically controlled position. Taking this into account, at lower levels of conversion, and if there are not geometrical constrains, one should expect a higher selectivity to the 1-AMN isomer. However, when contact time increases, not only does conversion increase, but also selectivity to the 2-AMN isomer increases, owing to secondary reactions (17) which involve the protodeacylation of 1-AMN as well as the migration of the acetyl group from position 1 to the 6-position of 2-MN (see Fig. 1) by a transacetylation mechanism. This reaction scheme and the influence of the level of conversion on product selectivity imply that the behavior of catalysts for the acylation of 2-MN should be compared at a similar level of conversion.

In the first part of our work, we have tested a series of zeolites with different pore dimensions, some of them with 12-MR pores, which were already used in previous works (USY and Beta), and others with 12 × 10 MR pores and 14-MR pores that have not been tested before (SSZ-33, UTD-1). The characteristics of these zeolites are given in Table 1. The results (Fig. 2) clearly show that while all of them were active, USY and UTD-1 zeolites, which have the largest pores, show very low selectivity to the 2-AMN isomer, since the most kinetically favored 1-AMN is almost exclusively formed, even at very high levels of conversion. On the other hand, Beta, as well as SSZ-33, was more selective toward the formation of the desired isomer, even if they were less active (lower level of conversion). Notice that SSZ-33, which can be considered to be formed by large and empty volumes (generated at the crossing points of 12- and 10-MR pores) connected to one another by either 12-MR or 10-MR windows, gives a slightly lower activity than Beta, but with a good selectivity to 2-AMN. The diameter of the 12-MR pores in SSZ-33 is 7.0 × 6.4 and 6.8 × 6.8 Å, while that of the 10-MR pores is 5.1 × 5.1 Å. Thus, it appears that diffusion of both acylated isomers can occur through the 12-MR pores of this zeolite. However, when the products are formed inside those empty volumes, 2-AMN can diffuse faster than the bulkier 1-AMN. Consequently, 1-AMN will spend more time before diffusing out, and in this time the consecutive protodeacylation and transacylation may occur, increasing the observed selectivity to the

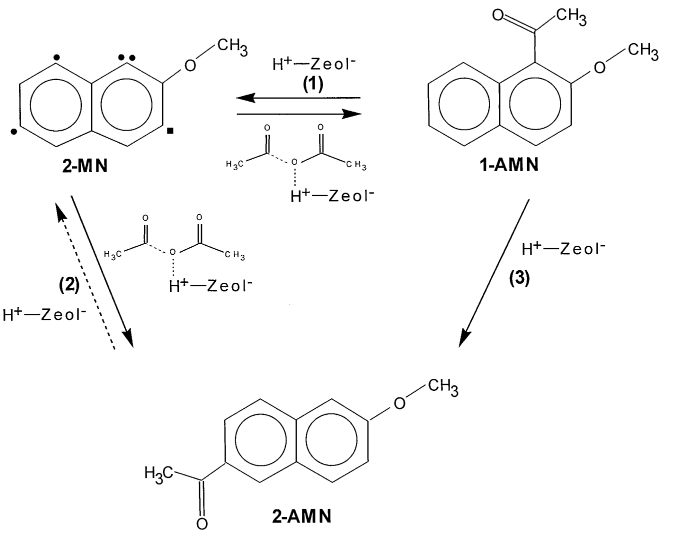

FIG. 1. Reaction scheme of the acylation of 2-MN with acetic anhydride over zeolites and possible secondary reactions over the acylation products. ● ●, Most activated position for the electrophillic substitution on 2-MN; ●, activated position; ■, low activated position; (1) protodeacylation of 1-AMN; (2) protodeacylation of 2-AMN. The dashed line indicates the lower probability of this secondary reaction due to the high thermodynamic stability of 2-AMN. (3) Transacylation of 1-AMN to 2-AMN.

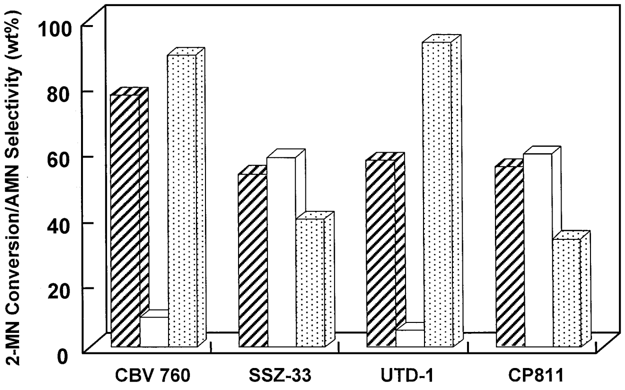

FIG. 2. Acylation of 2-MN with acetic anhydride over different zeolites. Conversion of 2-MN (▨) and selectivities to 2-AMN (□) and 1-AMN (⬚). Experimental conditions: $T = 405$ K; TOS = 4 h; 2-MN/AA = 2 : 1 (M); Cat/AA = 1 g : 20 mmol.

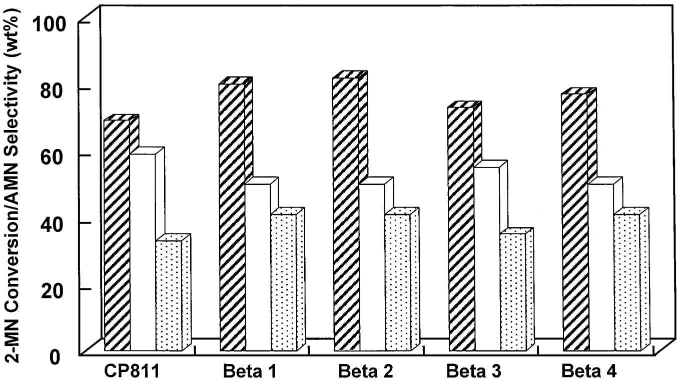

FIG. 3. Acylation of 2-MN with acetic anhydride over H-BEA zeolites. Conversion of 2-MN (▨) and selectivities to 2-AMN (□) and 1-AMN (░). Experimental conditions: $T = 405$ K; TOS = 4 h; 2-MN/AA = 2 : 1 (M); Cat/AA = 1 g : 10 mmol.

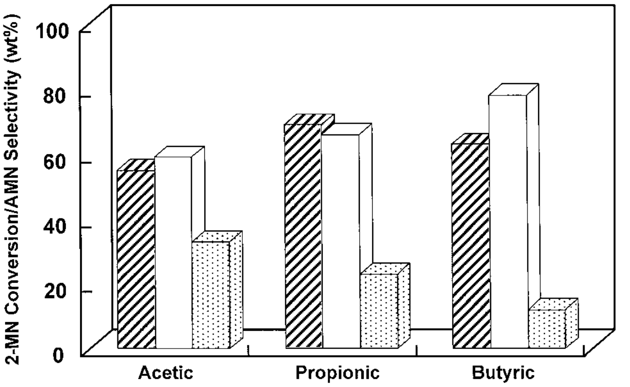

FIG. 4. Acylation of 2-MN with acid anhydrides of variable carbon chain lengths (two to four carbons) over H-BEA CP811. Conversion of 2-MN (▨) and selectivities to 2-AMN (□) and 1-AMN (░). Experimental conditions: $T = 405$ K; TOS = 4 h; 2-MN/AA = 2 : 1 (M); Cat/AA = 1 g : 20 mmol.

2-AMN product. Nevertheless, since Beta gave the best results, it was selected as the reference zeolite against which to compare the behavior of Al-ITQ-7. However, before this we decided to optimize the Beta zeolite from the point of view of the framework composition and crystallite size. To do this, Beta samples were prepared in our laboratory with Si/Al framework ratios of 25, 50, and 93, all with a crystallite size of 0.3–0.5 μm (Beta 1, 2, and 4 samples in Table 1). The acylation results given in Fig. 3 show that after 4 h of reaction, conversion was maximum for the samples with a 25 and 50 Si/Al ratio, while selectivity was similar in all cases.

For a reaction such as the 2-MN acylation in which one of the isomers is bulkier than the other and, consequently, its diffusion out of the channels is much slower, the sizes of the crystallites can play an important role on the product selectivity observed for two reasons. First, by decreasing the crystallite size of the zeolite the probability for the bulkiest product to be formed on the external surface strongly increases. Second, the pore length decreases and consequently the diffusion coefficient for the bulkier product (1-AMN) increases proportionally more. Both concepts lead to the same conclusion, i.e., when decreasing zeolite crystallite size the selectivity for the bulkier product should increase. Table 2 shows indeed that when working at low levels of conversion (11%), in order to avoid consecutive reactions, the reaction rate increases when decreasing the crystallite size from 1–2 μm (Beta 3 sample in Table 1) to 0.3–0.5 μm (Betas 1, 2, and 4 in Table 1 and 2), and the selectivity to 2-AMN decreases. These results are consistent, but do not say whether 1-AMN is formed exclusively on the zeolite surface or also inside the pores of Beta. At this point, we decided to carry out the acylation of 2-MN using anhydrides with different chain lengths. Results in Fig. 4 show that the selectivity to the 1-AMN product decreases

TABLE 2

Acylation of 2-Methoxynaphthalene with Acetic Anhydride over Al-ITQ-7 and Comparison with H-Beta Zeolites: Initial Rates for the Different Isomers Detected[a]

Catalyst	X_T 2-MN wt%[b]	X_T 2-MN wt%[c]	$r_{2\text{-AMN}}$[d]	$r_{1\text{-AMN}}$[d]	$r_{\text{Other AMN}}$[d]	$S_{2\text{-AMN}}$[e]	$S_{1\text{-AMN}}$[e]	$S_{\text{Other AMN}}$[e]
CP811	14	69	16.83	15.39	0	1.09	0.91	0
Beta 1	10	80	20.57	26.45	0	0.78	1.29	0
Beta 2	11	84	26.45	32.33	0	0.82	1.22	0
Beta 3	11	73	11.70	9.76	0.98	1.09	0.77	0.04
Beta 4	17	77	47.02	49.96	0	0.94	1.06	0
Al-ITQ7	15	40	11.64	6.4	0	1.82	0.55	0
Al-ITQ7n	10	28	4.11	7.64	0	0.54	1.86	0

[a] Experimental data: solvent, chlorobenzene; $T = 405$ K; catalyst/Ac_2O = 1 g : 10 mmol; 2-MN/AA = 2 : 1 (M).

[b] Conversion data considered for the calculation of the reaction rates.

[c] Maximum conversion reached at 4 h of reaction.

[d] Initial reaction rate in mmol g^{-1} h^{-1}.

[e] Kinetic selectivity indicated as the ratio between the reaction rate for a determinated product and the rates for the rest.

as the length of the anhydride chain increases. Then, if the bulkier 1-AMN was formed solely on the external surface we should not observe the selectivity to 1-AMN to decrease but, if anything, to increase in the case that the isomer acylated in position 6 starts to have problems forming inside the pores and the rate of reaction decreases. Therefore, we conclude that the formation of the 1-AMN product in Beta takes place not only on the external surface of the zeolite but also within the 7.2 × 6.2 Å pores.

From the above study of the acylation reaction with zeolite Beta, we have selected as a reference catalyst the Beta 3 sample with a Si/Al framework molar ratio of 50 and crystallite size of 1–2 μm. Then, a sample of Al-ITQ-7 with a Si/Al ratio of 50 and a crystallite size between 1 and 2 μm was prepared and the results obtained at different times are presented in Fig. 5a. The initial rate of the reaction was calculated from the slope of the curve of conversion versus time, when reaction time goes to zero. An analogous methodology was followed for the Beta 3 sample (Fig. 5b). The initial reaction rate (Table 2) indicates that Al-ITQ-7 is as active as Beta. Moreover, from the evolution of conversion with reaction time (Fig. 5) it is also evident that Al-ITQ-7 decays much faster. This is not surprising if one takes into account that the pores in Al-ITQ-7, by being smaller, will be more easily plugged by residual hydrocarbons. In order to see this, both catalysts, Beta and Al-ITQ-7, were taken after being used for 4 h and then washed and finally soxhlet-extracted. The residual amount of coke within the pores which could not be extracted was determined by thermogravimetric and elemental analysis to be 6.1 and 5.5, respectively, for Beta and Al-ITQ-7. The results show that a similar amount of hydrocarbons remain adsorbed in Al-ITQ-7 even at a clearly lower maximum conversion. The UV-visible analysis of the deactivated catalyst showed (Fig. 6) the typical bands of acetophenones and polyaromatics at 245–260 and 290–300 nm, respectively.

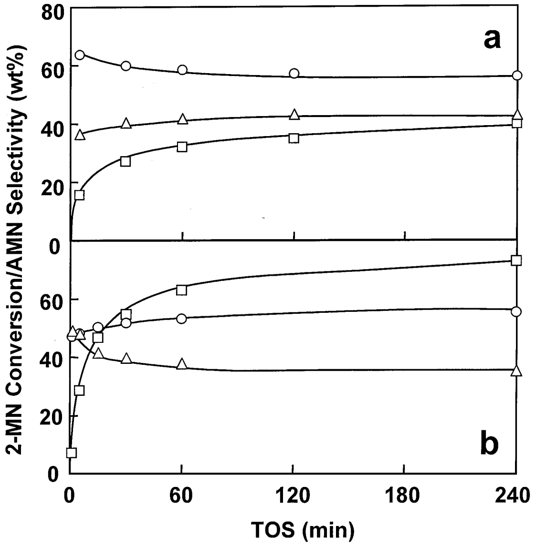

FIG. 5. Acylation of 2-MN with acetic anhydride over Al-ITQ-7 (a) and Beta 3 (b) samples (Si/Al = 50, catalyst average crystal size, 1–2 μm). Conversion of 2-MN (□) and selectivities to 2-AMN (○) and 1-AMN (△). Experimental conditions: $T = 405$ K; 2-MN/AA = 2 : 1 (M); Cat/AA = 1 g : 10 mmol.

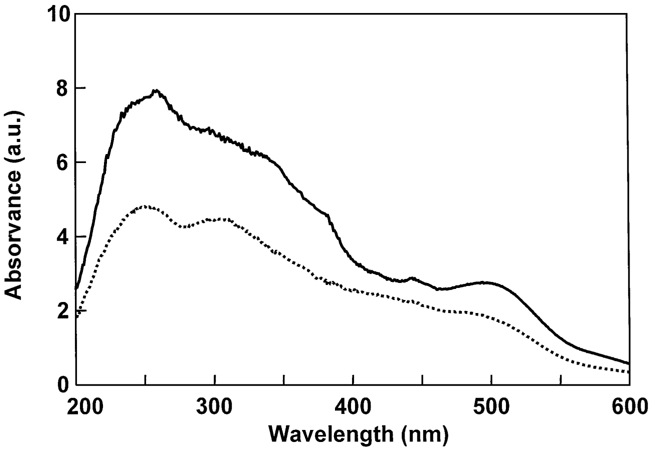

FIG. 6. UV-VIS spectra of Beta 3 (solid line) and Al-ITQ-7 (dashed line) samples (Si/Al = 50; catalyst average crystal size, 1–2 μm) after their use in the acylation of 2-methoxynaphthalene with acetic anhydride. Experimental conditions: temperature = 405 K; TOS = 4 h; Cat/AA = 1 g : 10 mmol; 2-MN/AA = 2 : 1 (M).

The selectivity of the two zeolites has been compared from the initial reaction rates for the formation of the different isomers, and the results show that the ratio for 2-AMN to the other products formed is 1.09 for the best Beta and 1.82 for Al-ITQ-7. This is clear proof that the pores of Al-ITQ-7, by being smaller than those of Beta, give a better shape selectivity effect for the formation of 2-AMN. This selectivity effect clearly disappears when the size of crystallites of Al-ITQ-7 is decreased from 1–2 to 0.02–0.05 μm (Table 2). Thus, it appears that the improved selectivity to 2-AMN with Al-ITQ-7 can be due to product diffusion shape selectivity.

In order to study the changes in the diffusion coefficients for the reactant 2-MN and the products when going from Beta to Al-ITQ-7, a Molecular Dynamics study was undertaken with these two zeolites.

In the case of Beta zeolite, Fig. 7 presents the trajectories of 1-AMN which indicate that the diffusion occurs through the *x*-direction (Fig. 7a) and through the *y*-direction (Fig. 7b). The distance traveled by the 1-AMN molecule is not very large, and in any case the molecules diffuse in either direction but none of the molecules is observed to change from one channel to another by passing through the channel intersection. This is probably due to the large size of the naphthalene ring which precludes the dihedral folding needed to follow the center of the void space in the rotation of 90° when changing from one channel along [010] to a channel along [100] or vice versa.

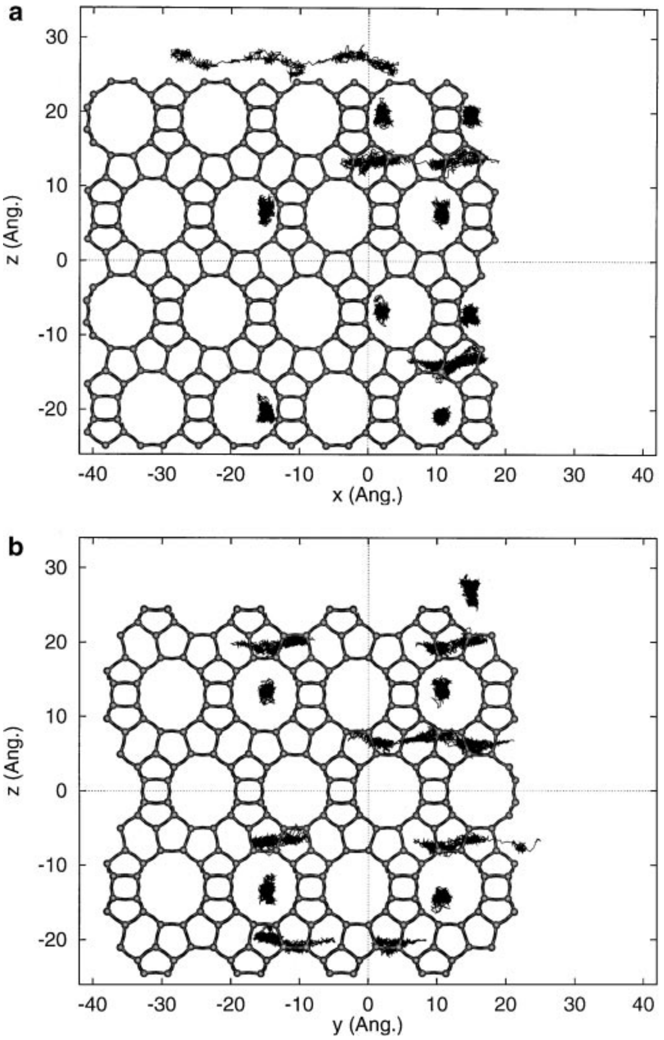

FIG. 7. Trajectories of the center of mass of the 13 1-AMN molecules diffusing through the Beta structure at 450 K. Projections in "*xz*" (a) and "*yz*" (b) are shown. The 12-MR channels of dimensions 7.2 × 6.2 Å which run parallel to [100] and [010] are shown.

The diffusion path of 2-AMN in Beta is similar, in the sense that no diffusion from one channel to another is observed, but nevertheless the trajectories in this case are longer due to the smaller size of this isomer. This fact is reflected in the corresponding diffusion coefficients (Table 3) and will be discussed later. Same considerations apply for the smaller 2-MN reactant molecule.

TABLE 3

Diffusion Coefficients Obtained from the Plots in Fig. 10[a]

Sorbate	Beta	ITQ-7
2-MN	21.71	5.88
2-AMN	10.44	3.87
1-AMN	3.90	0.25

[a] Diffusion coefficient (10^{-6} cm^2 s^{-1}).

In the case of Al-ITQ-7, the diffusion of 1-AMN through the channels is presented in Fig. 8, which shows that the molecules remain very close to the initial starting point through the 400-ps simulation. It appears then that the diffusion is very restricted in all channels and an "extensive local motion" appears. This behavior is in marked contrast with the diffusion of the same sorbate in the Beta zeolite (Fig. 7). It is clear that the slightly smaller size of the channels of ITQ-7 with respect to those of Beta is the reason for the observed difference. The size of the channels of ITQ-7 are (2×) 6.2 × 6.1 and (1×) 6.3 × 6.1 Å, while the channels of Beta are (2×) 7.2 × 6.2 and (1×)

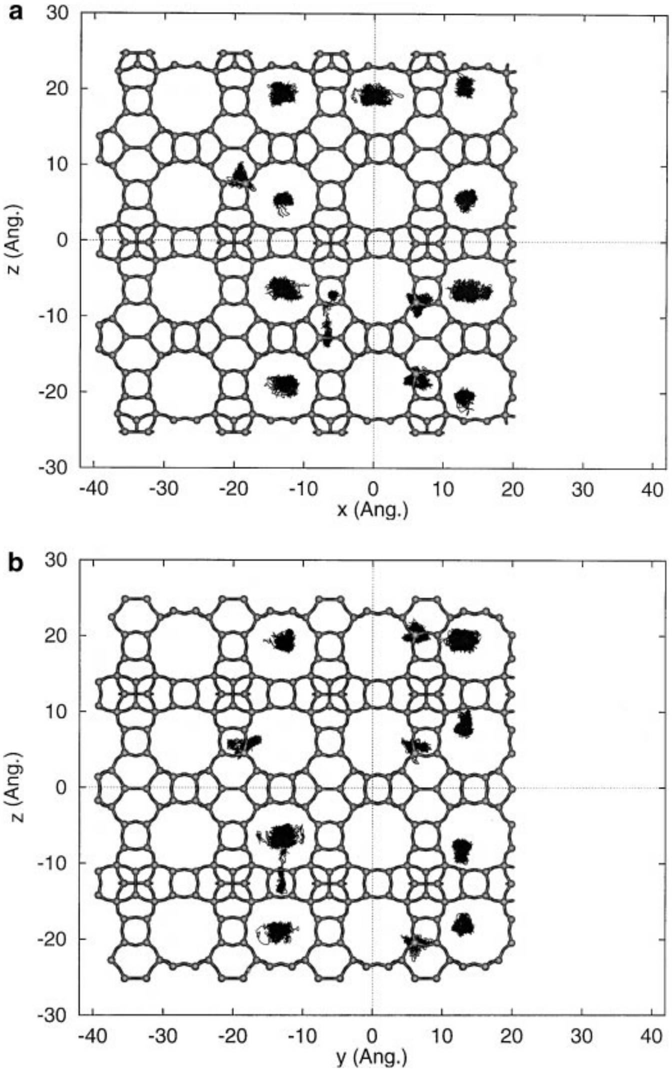

FIG. 8. Trajectories of the center of mass of the 13 1-AMN molecules diffusing through the ITQ-7 structure at 450 K. Projections in "*xz*" (a) and "*yz*" (b) are shown. The 12-MR channels of dimensions 6.2 × 6.1 Å which run parallel to [100] and [010] are shown. A third system of 12-MR channels of dimensions 6.3 × 6.1 Å runs parallel to [001].

5.5 × 5.5 Å. It follows that, although the third channel is wider in ITQ-7 than in Beta, the other two channels (running through [100] and [010]) are larger in Beta and this makes it easier for 1-AMN to diffuse. It was recognized early on that when the sizes of the sorbate and the zeolite void system are similar, small variations in the sorbate size can change the diffusivity by several orders of magnitude (46). Although this is not the case here, as will be seen from the diffusion coefficients below, it is quite clear that a slightly smaller pore size is, for the 1-AMN molecule, a strong impediment to diffuse. Results from Fig. 8 also indicate that diffusion is only observed along the [001] direction in ITQ-7. This is better seen (Fig. 8b) in the molecule located around $(y, z) \approx (-15, -7)$. This motion corresponds to the channel of 6.3 × 6.1 Å, which is the largest of the three channels of ITQ-7 if one considers the larger dimension of the opening the effective channel size. This consideration also explains the better diffusion of 1-AMN in Beta (Fig. 7), where the larger dimension of the opening through which the molecule diffuses is 7.2 Å.

Looking at the diffusion of 2-AMN in ITQ-7 we see much wider trajectories as correspond to the smaller size of this isomer (Fig. 9). The diffusion here is wider in two senses: first because of the larger distance traveled through the [001] channels and second because the channels through [100] and [010] are also used for diffusion. This makes the ITQ-7 a structure in which the three channels can be used for the diffusion of 2-AMN. This was not possible in the case of Beta because of the smaller size of one of the channels (5.5 × 5.5 Å). The case of 2-AMN diffusing in ITQ-7 shows another unique feature in the sense that some molecules are observed to change from one channel to another (see Figs. 9a and 9b). This is facilitated by the wide space available at the intersection between the channels in ITQ-7, which makes it possible for the bulky and rigid naphthalene unit to change its direction 90° without excessive repulsive proximity to the channel walls.

The diffusion coefficients for 2-MN, 1-AMN, and 2-AMN in Beta and ITQ-7 from the MD simulations are obtained from the MSD with Eq. [2]. The MSD plots are shown in Fig. 10, and the corresponding diffusion coefficients are shown in Table 3. The linearity of all the plots in Fig. 10 is a confirmation of the sufficient sampling reached in the MD simulations.

A comparison of the structural effect shows that all the diffusion coefficients for a given sorbate are larger in Beta than in ITQ-7. As mentioned earlier, the sorbates find two accessible channels in Beta of 7.2 × 6.2 Å, and a channel of 6.3 × 6.1 Å for the case of 1-AMN, and two additional channels of 6.2 × 6.1 Å for the cases of 2-AMN and 2-MN, in ITQ-7. From this, a possibility of a larger diffusion of 2-AMN and 2-MN in ITQ-7 with respect to Beta could be envisaged. However, the larger size of the available channels in Beta is more important than the number of channels and this justifies the larger diffusivity in Beta than in ITQ-7. A different behavior could be expected at higher loadings, where the effect of the larger void space of ITQ-7 may overcome the diffusion limiting factor of smaller channel sizes.

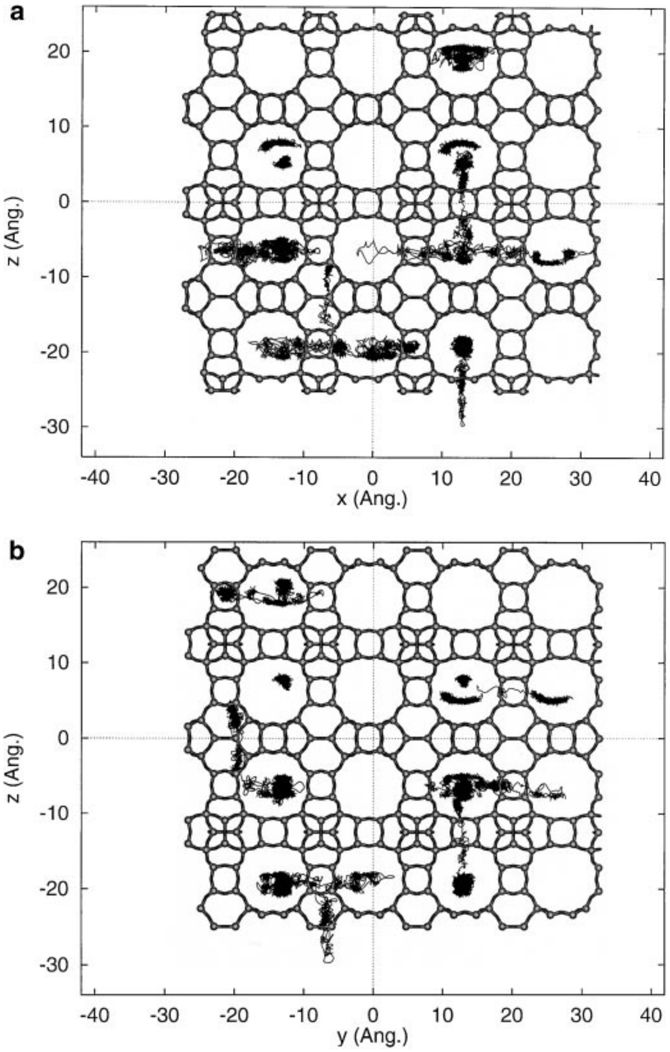

FIG. 9. Trajectories of the center of mass of the 13 2-AMN molecules diffusing through the ITQ-7 structure at 450 K. Projections in "*xz*" (a) and "*yz*" (b) are shown. The 12-MR channels of dimensions 6.2 × 6.1 Å which run parallel to [100] and [010] are shown. A third system of 12 MR channels of dimensions 6.3 × 6.1 Å runs parallel to [001].

A comparison of the sorbate size gives decreasing diffusion coefficients as the sorbate size increases (2-MN > 2-AMN > 1-AMN). The trend is not the same over the two structures and, for example, similar factors (2.1 and 1.5) are found between the relative diffusion coefficients of 2-MN and 2-AMN in Beta and ITQ-7, respectively, whereas very different factors (2.7 and 15.5) are obtained for the relative diffusion coefficients of 2-AMN and 1-AMN in Beta and ITQ-7, respectively. The reason for the large difference between the diffusion coefficients of 2-AMN and 1-AMN in

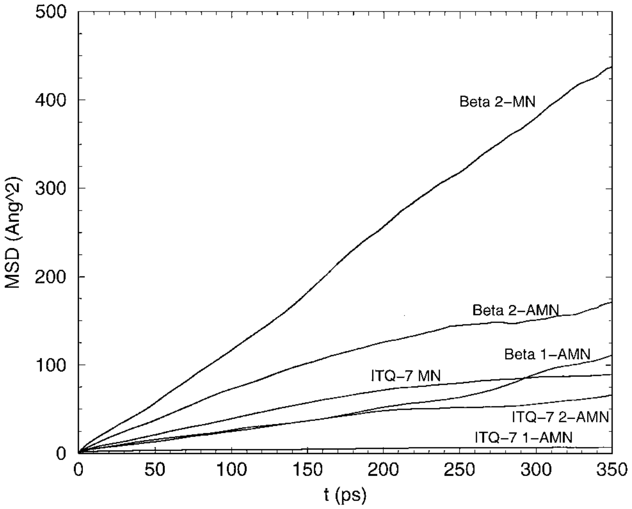

FIG. 10. Mean square displacements for 2-MN, 2-AMN, and 1-AMN in Beta and ITQ-7 zeolites. The diffusion coefficients obtained according to Eq. [2] (see text) are shown in Table 3.

ITQ-7 can be found in the fact that 2-AMN uses three channels whereas the 1-AMN uses only one channel. This fact confirms that a higher selectivity to 2-AMN can be expected in ITQ-7 than in Beta during the acylation of 2-MN with acetic anhydride.

CONCLUSIONS

Zeolite Al-ITQ-7, a tridirectional zeolite with some smaller channels than Beta, is active for the acylation of 2-methoxynaphthalene with acetic anhydride, giving a higher selectivity to the desired 2-acetyl-6-methoxynaphthalene than that obtained with Beta. It has been shown by Molecular Dynamics calculation that this is due to the much lower diffusion coefficient of 1-AMN in Al-ITQ-7 than in Beta.

By using anhydrides of different molecular sizes it has been shown that, at least in the Beta zeolite, the bulkiest isomer is formed not only on the external surface but also within the pores of the zeolites. In general, a decrease in crystallite size increases the reaction rate but decreases the selectivity to the less bulky and more desired 2-AMN. An efficient way to remove the surface acid sites without blocking the pore mouths combined with the use of Beta or Al-ITQ-7 with small crystallites should maximize both conversion and selectivity to 2-AMN.

ACKNOWLEDGMENTS

The authors thank the Comisión Interministerial de Ciencia y Tecnología in Spain (Project MAT 97-0561 and MAT 97-1016-C02-01) for financial support and the Centro de Investigaciones Energeticas, Medio Ambientales y Tecnologicas for the use of their computing facilities.

REFERENCES

1. Kuroda, C., *Sci. Papers Phys. Chem. Res.* **18**, 51 (1932).
2. Corma, A., *Chem. Rev.* **95**, 559 (1995).
3. Spagnol, M., Gilbert, L., and Alby, D., *Ind. Chem. Libr.* **8**, 29 (1996).
4. Fang, R., Harvey, G., Kouwenhoven, H. W., and Prins, R., *Appl. Catal. A General* **130**, 67 (1995).
5. Corma, A., Climent, M. J., García, H., and Primo, J., *Appl. Catal.* **49**, 109 (1989).
6. Harvey, G., Vogt, A., Kouwenhoven, H. W., and Prins, R., *Proc. Int. Zeol. Conf. 9th* **2**, 363 (1993).
7. Rohan, D., Canaff, C., Fromentin, E., and Guisnet, M., *J. Catal.* **177**, 296 (1998).
8. Spagnol, M., Gilbert, L., Guillot, H., and Tirel, Ph-J., Patent PCT, Int. Appl. WO 97 48,665 (1997).
9. Gilbert, L., and Spagnol, M., Patent PCT, Int. Appl. WO 97 17,324 (1997).
10. Harvey, G., and Mader, G., *Collect. Czech. Chem. Commun.* **57**, 862 (1992).
11. Neuber, M., and Leupold, E. I., Eur. Pat. Appl. EP 459495 B1 (1991).
12. Yadav, G. D., and Krishnan, M. S., *Chem. Eng. Sci.* **54**, 4189 (1999).
13. Harvey, G., Binder, G., and Prins, R., *Stud. Surf. Sci. Catal.* **94**, 397 (1995).
14. Heinichen, H. K., and Hölderich, W. F., *J. Catal.* **185**, 408 (1999).
15. Gunnewegh, E. A., Gopie, S. S., and van Bekkum, H., *J. Mol. Catal. A Chem.* **106**, 151 (1996).
16. Bharathi, P., Waghmode, S. B., Sivasanker, S., and Vetrivel, R., *Bull. Chem. Soc. Jpn.* **72**, 2161 (1999).
17. Fromentin, E., Coustard, J. M., and Guisnet, M., *J. Catal.* **190**, 433 (2000).
18. Villaescusa, L. A., Barret, P. A., and Camblor, M., *Angew. Chem. Int. Ed.* **38**, 1997 (1999).
19. Corma, A., Díaz-Cabañas, M. J., and Fornés, V., *Angew. Chem. Int. Ed.* **39**, 2346 (2000).
20. Zones, S. I., and Nakagawa, Y., *Microp. Mater.* **3**, 547 (1994).
21. Freyhardt, C. C., Tsapatsis, M., Lobo, R. F., Balkus, K. J., Jr., and Davis, M. E., *Nature* **381**, 295 (1996).
22. Botella, P., Corma, A., López-Nieto, J. M., Valencia, S., Lucas, M. E., and Sergio, M., *Appl. Catal. A General* **203**, 251 (2000).
23. Lobo, R. F., and Davis, M. E., *Microp. Mater.* **3**, 61 (1994).
24. Chica, A., and Corma, A., *J. Catal.* **187**, 167 (1999).
25. Meier, W. M., Olson, D. H., and Baerlocher, Ch., "Atlas of Zeolite Structure Types," 4th ed. Elsevier, Amsterdam (1996). Also at http://www.iza-structure.org.
26. Shannon, D. F., *Math. Comp.* **24**, 647 (1970).
27. Gale, J. D., *J. Chem. Soc. Faraday Trans.* **93**, 629 (1997).
28. Berendsen, H. J. C., Postma, J. P. M., van Gunsteren, W., DiNola, A., and Haak, J. R., *J. Chem. Phys.* **81**, 3684 (1984).
29. Verlet, L., *Phys. Rev.* **159**, 98 (1967).
30. Demontis, P., Fois, E. S., Suffriti, G. B., and Quartieri, S. J., *Phys. Chem.* **94**, 4329 (1990).
31. Deem, M. W., Newsam, J. M., and Creighton, J. A., *J. Am. Chem. Soc.* **114**, 7198 (1992).
32. Sastre, G., Catlow, C. R. A., and Corma, A., *J. Phys. Chem. B* **103**, 5187 (1999).
33. Smith, W., and Forester, T. R., *J. Mol. Graph.* **14**, 136 (1996).
34. Allen, M. P., and Tildesley, D., "Molecular Simulation of Liquids," Oxford Univ. Press, Oxford, 1980.
35. Catlow, C. R. A., Freeman, C. M., Vessal, B., Tomlinson, S. M., and Leslie, M., *J. Chem. Soc. Faraday Trans.* **87**, 1947 (1991).
36. Oie, T., Maggiora, T. M., Christoffersen, R. E., and Duchamp, D. J., *Int. J. Quant. Chem. Quant. Biol. Symp.* **8**, 1 (1981).
37. Ditchfield, R., Hehre, W. J., and Pople, J. A., *J. Chem. Phys.* **54**, 724 (1971).

38. Shubin, A. A., Catlow, C. R. A., Thomas, J. M., and Zamaraev, K. I., *Proc. R. Soc. Lond. A* **446**, 411 (1994).
39. Sastre, G., Raj, N., Catlow, C. R. A., Roque-Malherbe, R., and Corma, A., *J. Phys. Chem. B* **102**, 3198 (1998).
40. Yashonat, S., Thomas, J. M., Nowak, A. K., and Cheetham, A. K., *Nature* **331**, 601 (1988).
41. Schrimpf, G., Schlenkrich, M., Brickmann, J., and Bopp, P., *J. Phys. Chem*. **96**, 7404 (1992).
42. Nicholas, J. B., Trouw, F. R., Mertz, J. E., Iton, L. E., and Hopfinger, A. J., *J. Phys. Chem*. **97**, 4149 (1993).
43. Auerbach, S. M., Henson, N. J., Cheetham, A. K., and Metiu, H. I., *J. Phys. Chem*. **99**, 10600 (1995).
44. Sastre, G., Catlow, C. R. A., Chica, A., and Corma, A., *J. Phys. Chem. B* **104**, 416 (2000).
45. Kouwenhoven, H. W., and van Bekkum, H., *in* “Handbook of Heterogeneous Catalysis” (G. Ertl, H. Knözinger, and J. Weitkamp, Eds.), Vol. 5, p. 2358. VCH, Weinheim, 1997.
46. Schröter, H. J., and Jüntgen, H., *in* “Adsorption Science and Technology” (A. E. Rodrigues, M. D. LeVan, and D. Tondeur, Eds.), NATO ASI E158. Kluwer, Dordrecht, 1988.